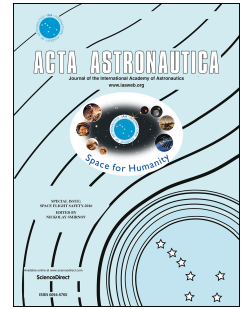


Journal Pre-proof

Rapid Prototyping of Satellite Shields: 3D Printed Carbon Fiber and Kevlar Composites for Hypervelocity Impact Protection

Stefano Lopresti, Leonardo Barilaro, Alberto Abiti, Lorenzo Olivieri



PII: S0094-5765(25)00530-2

DOI: <https://doi.org/10.1016/j.actaastro.2025.08.029>

Reference: AA 11366

To appear in: *Acta Astronautica*

Received Date: 2 July 2025

Revised Date: 5 August 2025

Accepted Date: 14 August 2025

Please cite this article as: S. Lopresti, L. Barilaro, A. Abiti, L. Olivieri, Rapid Prototyping of Satellite Shields: 3D Printed Carbon Fiber and Kevlar Composites for Hypervelocity Impact Protection, *Acta Astronautica*, <https://doi.org/10.1016/j.actaastro.2025.08.029>.

This is a PDF file of an article that has undergone enhancements after acceptance, such as the addition of a cover page and metadata, and formatting for readability, but it is not yet the definitive version of record. This version will undergo additional copyediting, typesetting and review before it is published in its final form, but we are providing this version to give early visibility of the article. Please note that, during the production process, errors may be discovered which could affect the content, and all legal disclaimers that apply to the journal pertain.

© 2025 Published by Elsevier Ltd on behalf of IAA.

Rapid Prototyping of Satellite Shields: 3D Printed Carbon Fiber and Kevlar Composites for Hypervelocity Impact Protection

Stefano Lopresti¹, Leonardo Barilaro², Alberto Abiti³, Lorenzo Olivieri⁴

¹ CISAS “G. Colombo”, University of Padova, Via Venezia 1, 35131 Padova PD, Italy – stefano.lopresti@phd.unipd.it

² Department of Aviation, The Malta College of Arts, Science & Technology, Triq Kordin, Paola PLA 9032, Malta, leonardo.barilaro@mcast.edu.mt

³ CISAS “G. Colombo”, University of Padova, Via Venezia 1, 35131 Padova PD, Italy – alberto.abiti@unipd.it

⁴ DII/CISAS, University of Padova, Via Venezia 1, 35131 Padova PD, Italy – lorenzo.olivieri@unipd.it

Abstract

This study explores the potential of 3D-printed composite shields for protecting satellites against hypervelocity impacts from space debris. Using a novel approach that integrates carbon fiber and Kevlar filaments, the paper presents a cost-effective and time-efficient methodology development for rapid prototyping satellite protection systems. Ten test samples were designed and manufactured implementing a dual-filament 3D printing process, employing carbon fiber as the primary structural material and Kevlar as the core. These shields were tested under simulated orbital collision conditions using a two-stage light-gas gun. The experimental results demonstrate the shields' effectiveness against hypervelocity impacts, revealing a significant correlation between manufacturing parameters and impact resistance. Preliminary results suggest that this methodology enables the development of customized, efficient shielding solutions with reduced production times and costs. A follow-up experimental campaign is outlined to further refine the technology, optimize the associated uncertainty range and assess its broader applications in space systems. This research contributes to the growing field of space debris mitigation, offering a promising approach to enhancing the resilience of orbital assets against collision threats.

Nomenclature

HVI: Hypervelocity Impact

EVA: Extravehicular activity

MRO: Maintenance, Repair, and Overhaul

MMOD: Micrometeoroids and Orbital Debris

FFF: Fused Filament Fabrication

CFRP: Carbon Fiber Reinforced Polymer

SPH: Smoothed-Particle Hydrodynamics

TRL: Technology Readiness Level

DPI: Dots Per Inch

V_{res} : Residual velocity of the debris cloud

V_{Rad} : Radial velocity of the debris cloud

D_c : Debris Cloud Diameter

Beta: Debris Cloud angle with respect to the plate

l_c : Debris Cloud horizontal extension

V_x : Mean x velocity of the fragments

V_y : Mean y velocity of the fragments

t_d : Time at which a fragment is detected for the first time

1. Introduction

The aerospace sector is undergoing a significant transformation, marked by the rapid growth of the small satellite market and the reduced launch costs democratizing the access to space [1]. This evolution is boosting the adoption of innovative technologies from terrestrial industries, that previously were only moderately adapted for space applications. Among these, additive manufacturing, or 3D printing, is emerging as a revolutionary tool for designing and producing satellite components. Its capacity to create complex geometries, optimize material properties, and drastically cut prototyping time and costs makes it uniquely suited to the demands of the modern space industry [2] [3]. In particular, additive manufacturing allows the design and implementation of novel and high-performance solutions, that can be easily adapted to different mission profiles and requirements [4] [5] [6].

In parallel, the current proliferation of orbital debris poses an escalating and critical threat to the sustainability of space operations. With more than 50,000 pieces of debris being tracked and catalogued in Earth orbits and more undetected, the risk of hypervelocity impacts (HVIs) on active satellites and crewed spacecraft is rising [7]. This threat creates a dual challenge. First, there is the clear need to equip new satellites with increasingly efficient shields without affecting the spacecraft mass budget (and, consequently, the launch cost). Second, it is necessary to develop a viable strategy to repair damages sustained by long-duration missions, such as orbital stations like the ISS. Traditionally, repairing a damaged shield is a logistically complex and expensive operation, often necessitating the transport of large replacement panels and high-risk EVAs (Extravehicular activities).

One of the most promising applications is the development of 3D-printed repair patches for aerospace structures damaged by high-energy impacts [8] [9]. The ability to produce such elements directly in orbit could revolutionize maintenance, repair, and overhaul (MRO) procedures for space assets, significantly reducing costs and risks. In particular, this study proposes a novel methodology to accelerate the development of such systems, integrating advanced simulation techniques with practical, cost-effective rapid prototyping. These innovations can enhance the effectiveness of protective systems while minimizing weight and volume, addressing critical challenges in space engineering [10] [11].

The remainder of this paper presents a preliminary experimental campaign focused on 3D-printed shields composed of a carbon fiber structure and a Kevlar core. Ten samples were tested under simulated orbital collision conditions to assess the correlation between manufacturing parameters and impact resistance. The results propose a new, streamlined development pathway for customized shielding solutions, aiming to prove the concept and pave the way for a new generation of more efficient and sustainable protection for orbital spacecraft.

2. State of the Art

Rapid prototyping is crucial in satellite development for accelerating innovation and reducing costs by enabling early identification of design flaws [12]. By iterating through designs quickly, engineers can validate new technologies and refine objectives before committing to full-scale production. This is particularly valuable for the growing number of universities, startups, and research teams entering the space sector. A promising field for the application of this methodology is the development of protective shields against micrometeoroids and orbital debris (MMOD). One of the bigger limitation of the current shields is the loss of protection capabilities after the collision with a MMOD in the entire region of the impact, and repair requires the complex and costly replacement of an entire panel, often involving an EVA. Additive manufacturing presents a transformative solution by enabling the possibility of printing repair patches directly in orbit [13]. These patches could be customized to the exact size of the damage, optimizing material usage and restoring the original structural integrity of the spacecraft [14].

The aerospace industry was an early adopter of 3D printing, primarily for prototyping [15]. Today, its use has expanded to include end-use parts, driven by advancements in printing flame-retardant and high-strength composite materials. Fused Filament Fabrication (FFF) is a popular method that has evolved to incorporate reinforcements like carbon fiber to enhance the mechanical properties of thermoplastics like ABS, PEEK, and Nylon. [16] Generally, for these applications the approach is to use short, chopped fiber filament immersed

50 in an epoxy matrix, although for high-performance applications, some continuous fiber structures have
51 recently begun to be printed between the layers to better distribute loads and increase mechanical
52 properties. The performance of FFF parts is highly dependent on process variables like raster angle, which
53 can induce orthotropic behavior, and achieving strong interlayer bonding to minimize voids.
54 Previous research, such as the H2020 ReDSHIFT project [17], has already demonstrated that 3D-printed
55 aluminum shields can be a valid alternative to traditionally manufactured ones, showing comparable ballistic
56 properties. This study builds on the foundation of the Smart Ballistic Optimization for Repairing of Aerospace
57 Exostructures using 3D printed Kevlar (SBORAEK) project, which developed ballistic-optimized, 3D-printed,
58 continuous-fiber shields for high-energy impact applications in aerospace [18].

59 **3. Methodology**

60 This study provides a methodology for the rapid development and prototyping of satellite shields and
61 reparative patches using 3D-printed carbon fiber reinforced polymer (CFRP) and Kevlar filaments.
62 The primary goal is to create and test a shield with a comparable mass to a traditional shield to evaluate its
63 impact survivability in a hypervelocity facility.

64 **3.1 Step by step development**

65 The development process was designed to be rapid, accessible, and iterative, ensuring the methodology is
66 affordable and simple to implement in any laboratory with (relatively) commonly available 3D printers and
67 materials. The process follows these key phases:

- 68
- 69 • A preliminary step was a review study of existing literature on canonical carbon fiber shields to establish
70 baseline parameters for thickness, manufacturing techniques, and previous test conditions. This was
71 done to ensure the newly designed samples would be directly comparable to existing solutions.
- 72 • An initial design phase was conducted using a multi-objective optimization procedure to evaluate
73 different geometries, masses, and expected failure thresholds. This was supported by coarse numerical
74 simulations using an SPH algorithm to identify thicknesses expected to provide a ballistic response
75 comparable to classical shields. This "simulation-first" approach is intended to shorten development
76 time by reducing the need for extensive and costly ground experiments.
- 77 • Based on the simulation results, test samples were developed and manufactured. The focus was on
78 creating fully functional and representative prototypes to achieve a proof-of-concept at Technology
79 Readiness Level (TRL) 5.
- 80 • The prototypes were subjected to a preliminary hypervelocity test campaign to assess their
81 performance under relevant conditions and validate the simulation models. Following the iterative
82 approach of this methodology, once consolidated with accessible materials, a second development
83 phase using more specialized materials and machinery can be undertaken. The data from the first test
84 campaign is intended to refine the simulation models, creating a more accurate "digital twin" that can
85 predict the performance of future designs and reduce the number of required physical tests.

86 The flowchart of the methodology is resumed in Figure 1. Following this philosophy that reflects the principles
87 of the concurrent engineering, it was possible to pass from the designing phase to the test in a reduced time,
88 anticipating the problems and minimizing the costs.

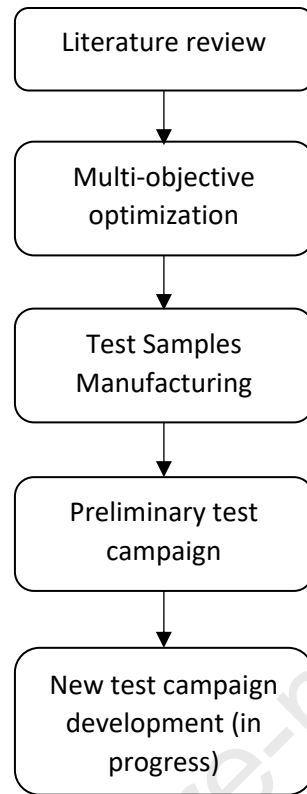


Figure 1: Flowchart of the methodology

89

90

91 3.2 Shields design

92 The shield design process is fundamentally driven by a hybrid simulation approach that combines empiric
 93 modeling with faster, scenario-based virtual testing.

94 The shields were produced with an Ultimaker S5 printer, chosen for its dual-nozzle capability, which is
 95 essential for printing with two different materials like carbon fiber and Kevlar that have different
 96 temperature and nozzle requirements (Figure 2). The printer's controlled environment and filament
 97 preservation system ensure precision and repeatability, even for samples printed weeks apart.

98 In Table 1 the selected printing parameters are reported

99

100

Table 1: Printing parameters

Process parameters	CFRP	Kevlar
Nozzle Diameter [mm]	0.8	0.4
Layer height [mm]	0.4	0.2
Print Speed [mm/s]	50	25
Print Temperature [C°]	280	260
Build plate temperature [C°]	65	//
Infill density [%]	Refer to Table 2	Refer to Table 2
Infill pattern	zig-zag	zig-zag

Built plate adhesion type	Brim	//
---------------------------	------	----

101

102

103

104

105

106

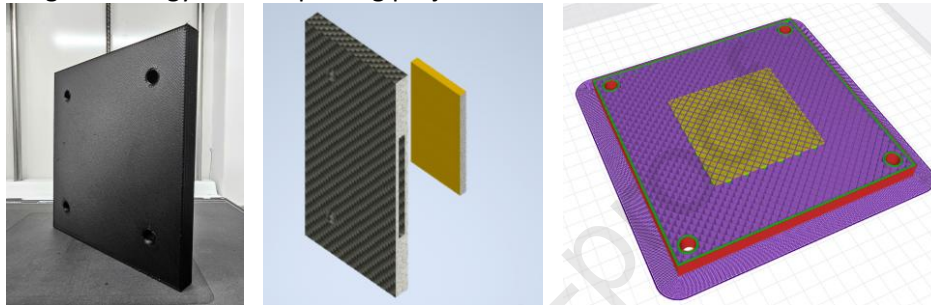
107

108

109

110

For the samples, the DoE matrix was designed to test the combination of two different materials: for the structure it was selected a polyamide matrix reinforced with short carbon fibers embedded in omnidirectional orientation. In particular the printing was performed with the “Luvocom Path CF 9891 BK”. For the core, instead, a Kevlar filament embedded in an ABS matrix manufactured by Kimya was chosen. The “Luvocom Path CF 9891 BK” has mechanical properties that are much lower than those of a carbon fiber panel, as the tensile strength is around 120MPa and the modulus of elasticity is 120GPa. Stiffness, however, is not the main property searched, and these parameters, combined with shock absorbing capabilities of Kevlar and ABS core, make it possible to have a panel that is rigid enough to be structural but capable of effectively dispersing the energy of an impacting projectile.



111

112

113

114

Figure 2: 3D-printed samples layout: On the left: Printed test sample. In the center: composition of the samples. The outer CFRP shell is shown in black, while the Kevlar core is shown in yellow. On the right: the path of the nozzle during printing

115

116

117

118

119

120

121

The samples produced are 150mm squares with holes for hanging in the laboratory test chamber. The Kevlar layer is only placed in the center of the test specimen, in a square of side 70mm (Figure 3). The nominal point of impact is the exact center of the sample, with the diameter of the impact tolerance area of 25mm. The total thickness of the target is 12mm, the thickness of the inner core is 6mm. In order to reduce weight, the shields were printed at low density, as shown in Table 2

Table 2: 3D-printed samples test matrix summary

Plate	Infill CFRP [%]	Infill Kevlar [%]	Configuration	Print direction	Impact Velocity [m/s]	Projectile material
0A (test)	8	20	Single wall	Vertical	4200.0	Aluminum
1	20	20	Single wall	Horizontal	2699.8	Aluminum
2	10	20	Single wall	Horizontal	4157.7	Aluminum
3	10	20	Single wall	Horizontal	4181.0	Aluminum
4	10	20	Single wall	Horizontal	4332.0	Aluminum
5	10	20	Single wall	Horizontal	5121.0	Aluminum
6	8	20	Multiple wall	Vertical	2755.4	Aluminum
7	10	20	Multiple wall	Vertical	4073.0	Aluminum
8	10	20	Multiple wall	Vertical	4920.7	Aluminum
9	10	20	Multiple wall	Vertical	5031.6	Steel
10	10	20	Multiple wall	Vertical	5250.8	Steel

122

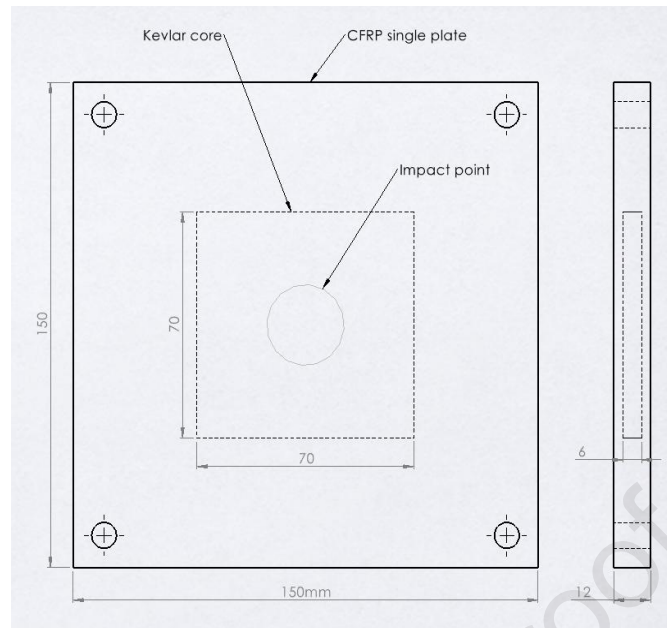
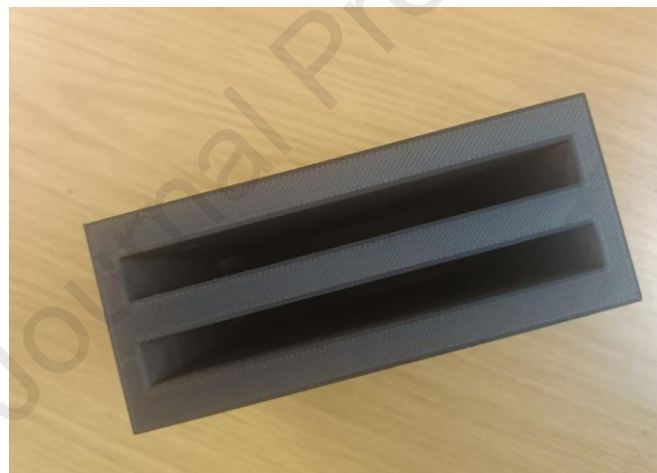


Figure 3: 3D-printed sample dimensions

123

124

125 For the test campaign, two sets of test samples were produced, a single-plate and a multi-plate structure,
 126 consisting of three single plates spaced 12mm apart (Figure 4).



127

128

Figure 4: Top view of the multiplate structures.

129 In order to investigate also the influence of the printing direction on the ballistic capabilities of the test
 130 samples, the plates were manufactured following two different printing orientations: the orientation will be
 131 called "horizontal" if the plates are produced with the major face facing the printing plate, will be called
 132 "vertical" if a plate is printed with one of the thin faces facing the printing plate. In this test campaign, all the
 133 single plates, except for the one used for the test shot, were printed horizontally, while all multiplate were
 134 produced vertically.

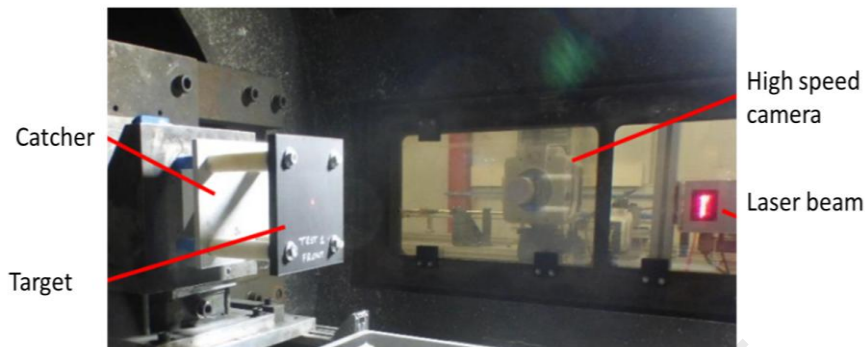
135

4. Test campaign

136 The test campaign consisted of 10 tests, plus a centering test. The first five tests and the centering shot were
 137 performed on single plates, using a 3 mm-diameter aluminum ball as a projectile with a velocity varying from
 138 3 to 5 a km/s. Tests 6 to 10, on the other hand, were performed on multiplate, using both aluminum and
 139 steel balls, at the same velocities.

140 The tests were performed with the 2-stage light gas gun "Hermes" in Thiot Ingegnerie's Shock Physics Lab
 141 (Figure 5). For the recording, a high-speed Phantom V2012 camera was placed at the side of the target to

142 capture images of the impact. Projectile speed is measured through the “VMS2000”, a system based on four
 143 optical fibers that allows velocity to be measured by occlusion of laser beams with a measurement error of
 144 less than 1%.



145

146 *Figure 5: Experimental setup. (Image courtesy of Thiot Ingegnerie)*

147 Behind each sample, at a distance of 100mm, a soft ballistic gel catcher was placed to stop the fragments
 148 and collect some additional data on the debris cloud. All soft catchers were sent to the Malta College of Arts,
 149 Science, and Tecnology (MCAST) after the test campaign and analyzed. An example of the catcher is shown
 150 in Figure 6; results regarding the generated fragments are still under evaluation

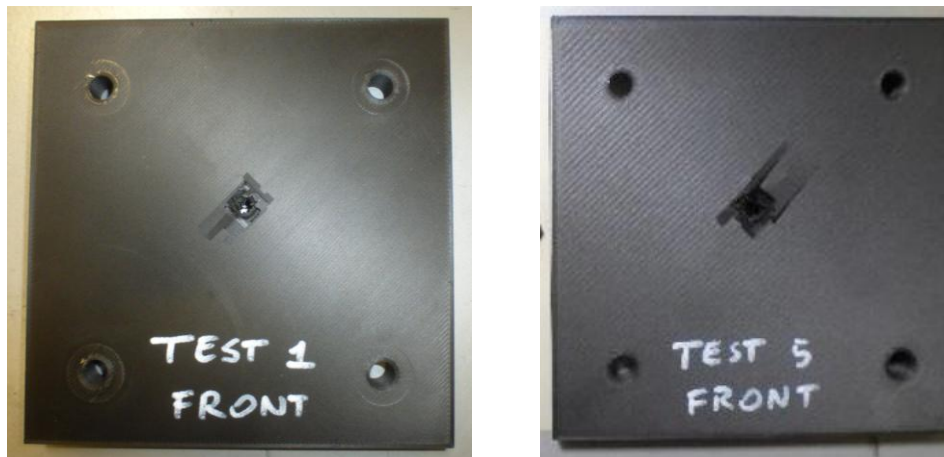


151

152 *Figure 6: Soft ballistic gel catcher placed behind the target*

153 **5. Test results**

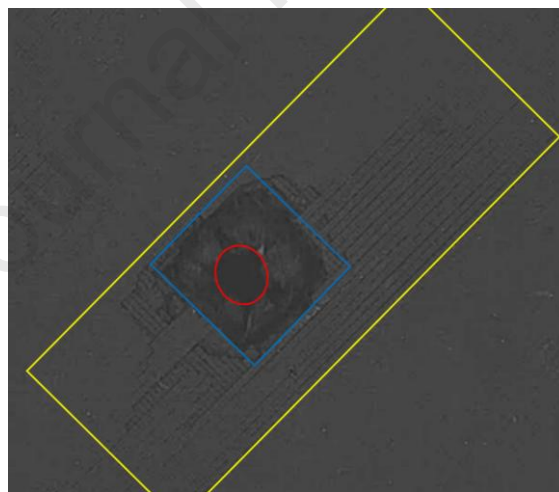
154 For each test, a projectile and sample weight measurement were taken before the test, and all samples were
 155 also weighed after the test. A photo of a plate after a test is shown in Figure 7



156

157 *Figure 7: Test 1 and Test 5 after impact. For the samples printed “horizontally” damage is localized and delamination*
 158 *of the first layers has been detected*

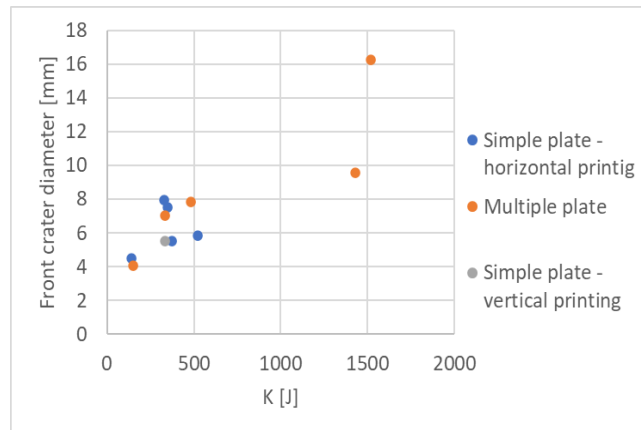
159 All plates were then scanned from both sides using a 600 DPI scanner and the images were analyzed using a
 160 Matlab™ procedure that calculates the hole area. This step is particularly delicate as the damage on
 161 structures of this composition is not circular as is usually the case with isotropic materials but has a more
 162 irregular shape. The code then associates an ellipse (red) with the hole to best describe its edges; the value
 163 shown in the following tables is the arithmetic mean between the two semi-axes. In addition, the code is able
 164 to detect the area in which the entire CFRP layer has been damaged, exposing the inner Kevlar layer (blue).
 165 Finally, in yellow is identified the total area in which there was a surface delamination of the first layer as a
 166 result of the impact (Figure 8).



167

168 *Figure 8: Graphic representation of the damaged area identifying the crater (red), the inner damage (blue) and the*
 169 *total delamination (yellow)*

170 The damage sustained by the 3D-printed shields, as measured using the described procedure, was compared
 171 across all the performed tests using an energetic parameter as the kinetic energy of the projectile. The
 172 following graph shows the crater size versus the kinetic energy of the impacting body (Figure 9).



173

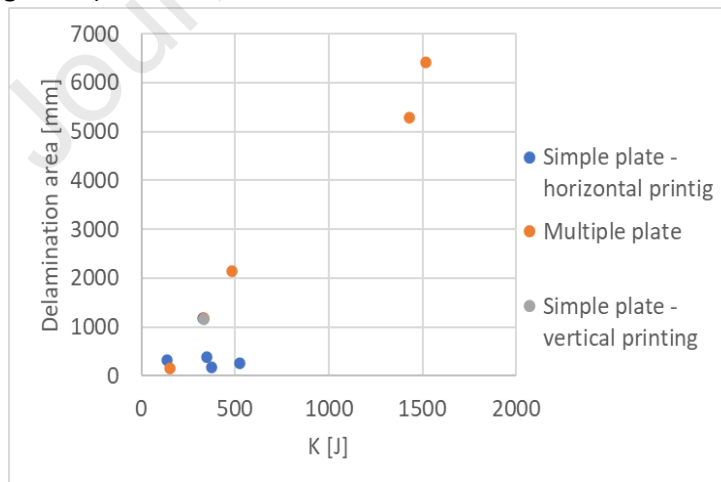
174

Figure 9: Front crater diameter in function of impactor kinetic energy.

175 This first campaign doesn't aim to have a sufficient number of tests to make relevant statistics, but to identify
 176 some trends to be studied through future dedicated campaigns; furthermore, given the scarcity of
 177 experimental data on such materials, the authors emphasize the importance of disseminating these data in
 178 the scientific literature.

179 In this case it is possible to observe a clear tendency for multiplate, while the distribution of impacts on single
 180 plates is more chaotic. This discrepancy is due to the different printing direction of the plates. As the filling is
 181 between 10% and 20% and the internal structure of the plate is reticular, the ability of the projectile to
 182 penetrate and the damage done depends on the impact position on the underlying reticle, this leads to an
 183 uncontrollable degree of freedom that make extremely complex to describe the curve's behavior
 184 mathematically. The situation changes when it comes to multiplate, since the velocity of motion is
 185 perpendicular to the direction of filling, the projectile encounters a material with more constant properties
 186 regardless of the actual point of impact.

187 With respect to surface delamination, the results seem to indicate that two different mechanisms
 188 drive in phenomena (Figure 10).

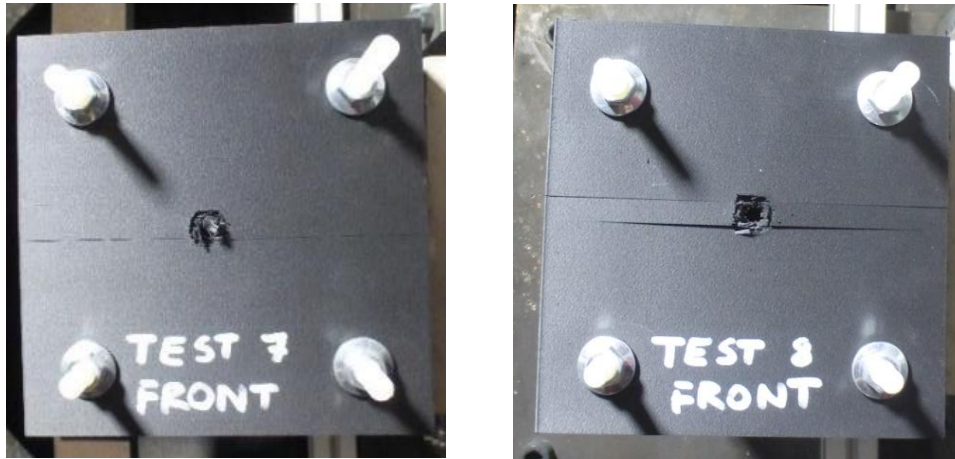


189

190

Figure 10: Total delamination area in function of impactor kinetic energy.

191 For single-plate structures, the entire surface is made of a single printing layer, which remains more cohesive
 192 and even as the impact energy increases, does not delaminate excessively. In vertically-printed structures,
 193 on the other hand, the projectile strikes several layers laterally, which offer less resistance and, in the case
 194 of high-energy impacts, can result in a fracture between the layers that can be several millimeters deep
 195 (Figure 11).



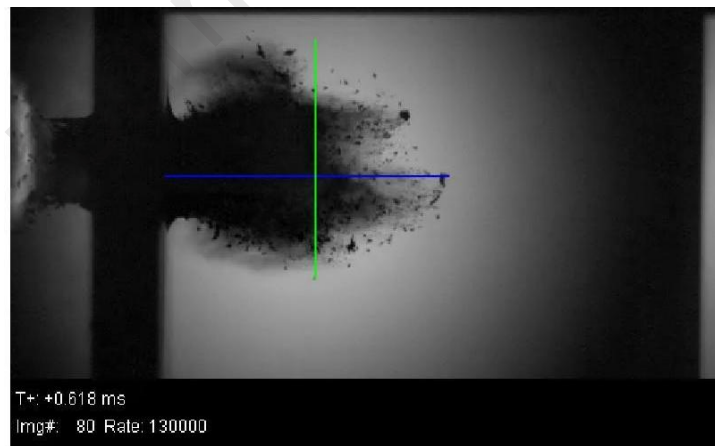
196

197 *Figure 11: Test 7 and Test 8 after impact. For the samples printed “vertically” a crack is triggered and propagates*
 198 *between the layers of printed material*

199 This is confirmed by the fact that the experimental point obtained with the test single plate, produced in the
 200 direction of the multiplate, aligns perfectly with the experimental points of the multiplate.

201 5.1 Cloud analysis

202 In addition, during the tests videos of the fragmentation were recorded using a Phantom v2012 ultrahigh-
 203 speed digital camera. In order to extract more information about the produced fragments and their time
 204 evolution, a video analysis of the produced debris cloud was performed using a Matlab™ code. As the first
 205 step, the code extracts the frames of the video showing the first moments of the cloud propagation. For each
 206 frame of interest, after binarizing the image and selecting manually the area including only the cloud, it
 207 automatically measures the horizontal (blue) and vertical (green) limits of the cloud, as shown in Figure 12.



208

209 *Figure 12: Cloud extension analysis for plate 2 fragmentation video*

210 At this point, it is possible to calculate the residual velocity of the cloud (V_{RES}), the radial velocity (V_{RAD}) and
 211 the values of the cloud diameter (d_C) and the angle (β), both measured at a specified value of the horizontal
 212 extension l_C . Results are summarized in Table 3. The measurements were possible only for single plates tests
 213 due to the insufficient number of frames showing the debris cloud before the impact with the rear wall of
 214 the multiple plate shields.

215

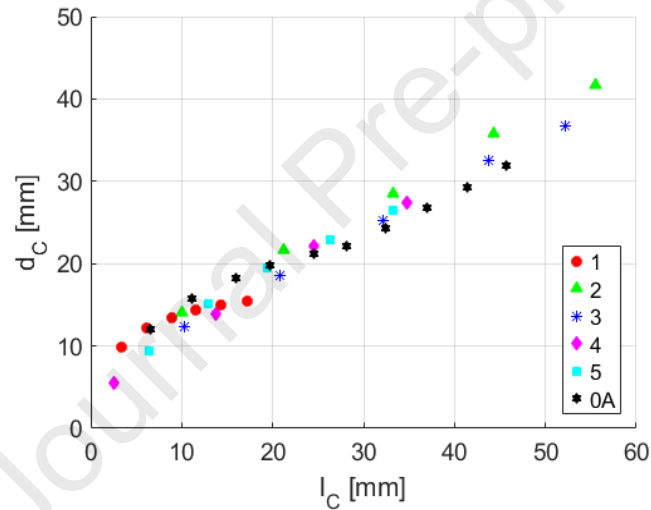
216

Table 3: Residual and radial velocities of the fragment clouds for single plate tests

Plate	V_{RES} (m/s)	V_{RAD} (m/s)
0A	562.3	139.1
1	687.6	273.5
2	1470.1	889.1
3	1350.3	784.9
4	2015.1	1360.9
5	1257.8	278.1

217

218 In contrast with the hole diameter in the front face, the evolution of the cloud appears to be very regular and
 219 the influence of the impact position seems absent. Below is the graph showing the coordinates of the
 220 longitudinal dimension and circumferential development of the cloud for the available frames. Interestingly,
 221 the points tend to align on the same curve (Figure 13).



222

223

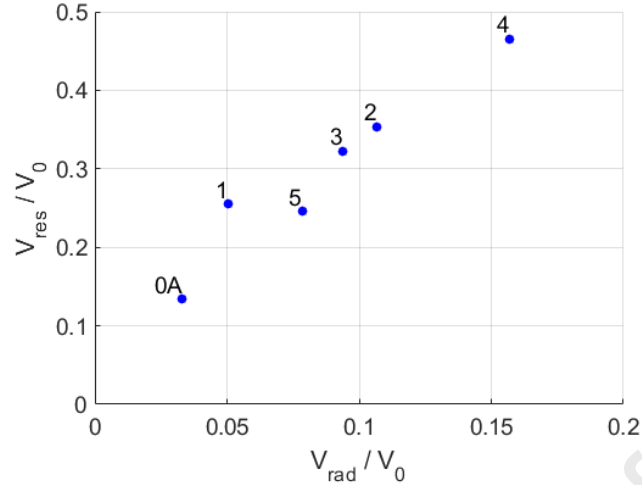
224

Figure 13: Cloud diameter extension as a function of the cloud horizontal extension.
 Different markers indicate the different simple plate tests

225

226

Plotting the radial and residual velocities of the normalized clouds against the initial velocities, it can be noted that these tend to respect constant ratios (Figure 14).



227

228

Figure 14: Ratio between VRES and the impact velocity V_0 as a function of the ratio between V_{RAD} and V_0 .

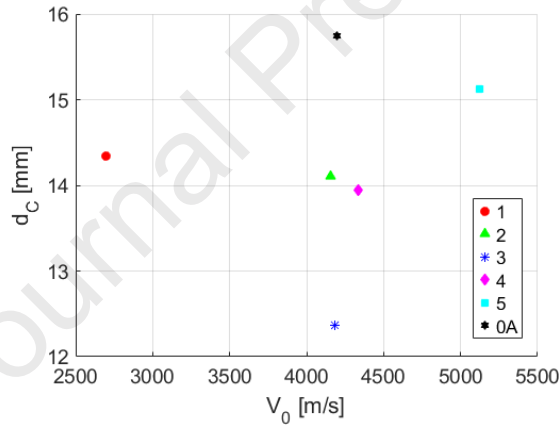
229

230

231

232

Furthermore, Figure 15 shows the value of d_c measured for $l_c = 11.61 \pm 2.00$ mm. The uncertainty of this value depends on the number of frames where the cloud extension was measurable. The plot suggests that in all tests, with the exception of test 3, d_c appears to have no significant variation over the uncertainty range, more data will be needed to confirm this hypothesis.



233

234

Figure 15: d_c measured for $l_c = 11.71 \pm 2.00$ mm as a function of V_0 .

235

5.2 Fragments velocity analysis

236

237

238

A further study was done by applying a Matlab™ procedure to the frames of the video to track the fragments and calculate their speed, instant by instant. The procedure can be divided into two main steps: the first part detects for each frame the center of mass and the area of the fragments as follows:

239

240

241

242

- The frame is converted to grayscale;
- The frame is binarized using an adaptive threshold;
- Adjacent pixels of the same type are connected to identify the fragment areas and their corresponding centers of mass.

243

244

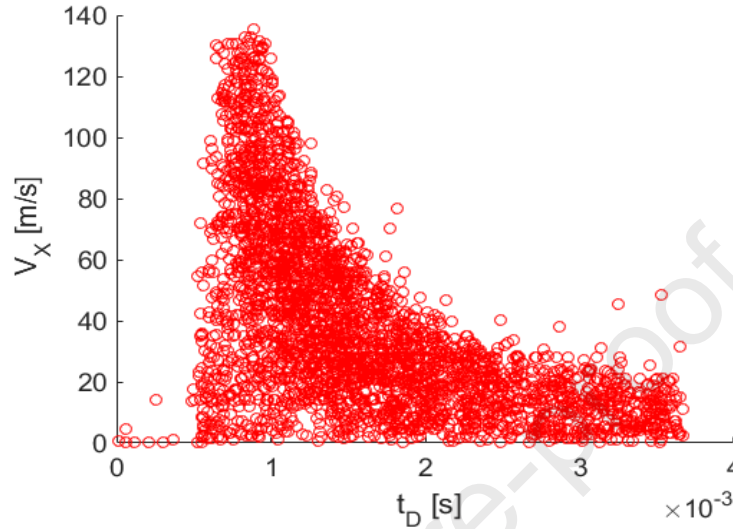
245

246

247

The second part identifies the fragment trajectories. Starting from the assumption that during the rapid evolution of the collision, the gravity effect on the fragments is negligible, the trajectories are considered to be straight lines. For this reason, a Random Sample Consensus (RANSAC) algorithm is applied to interpolate the detected centers of mass obtaining the straight trajectories. By overlaying the identified trajectories onto the video frames, the validity of this assumption can be confirmed.

248 From this procedure, it was possible to calculate various cinematic parameters of the fragments, such as their
 249 mean velocities in horizontal (V_x) and vertical (V_y) direction. Figure 16 presents a graph in which the time at
 250 which a fragment is detected for the first time (t_D) is shown in the abscissa and V_x is shown in the ordinate.
 251 t_D is assumed to be close enough to the time the fragment detached from the 3d printed plate. Fragment
 252 detection could be performed only for single plate tests, since multiplate tests showed no complete
 253 perforation or, as in test 10, there were not enough frames to complete the tracking.



254

255 *Figure 16: Fragments velocities in horizontal direction as a function of the time of the first frame in which they become*
 256 *visible for test 2.*

257 It can be observed that the detected fragment velocities uniformly populate a graph area outlined by a
 258 power-type curve, following equation (1)

259

$$V_x = A * t_D^B \quad (1)$$

260 The coefficients were determined through a non-linear fit and their values are reported in Table 4.

261

Table 4: Summary table of coefficients used

Test	A	B
0A	0.1886	-0.8184
1	0.0386	-0.9889
2	0.4547	-0.7175
3	0.2408	-0.8066
4	0.3263	-0.7023
5	0.2332	-0.7621

262 Finally, the curves, normalized by the initial velocity of the debris cloud V_{RES} , are represented in Figure 17.
 263 However, it must be noted that during the initial moments of the collision, capturing individual fragments is
 264 particularly challenging as the cloud appears as a single body. For these moments, the curves are
 265 approximated using the equations while the fragments velocities remain lower than the cloud velocity V_{RES}
 266 shown in table 2, and assuming a uniform velocity equal to V_{RES} when V_x exceeds that value.

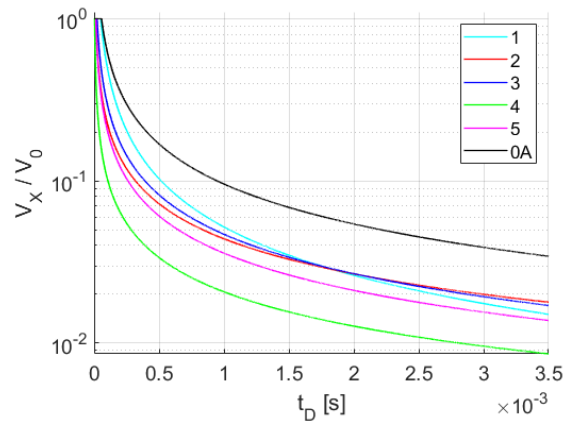


Figure 17: Representation of the curves outlining the fragment horizontal velocity distributions, normalized by the collision speed, as a function of the time of the first frame in which they become visible.

267

268

269

270 The subtended area, normalized by the initial velocity of the impactor, can suggest information about the
 271 absorption capacity of each plate. In particular, test 0A exhibits a higher curve compared to the others,
 272 indicating that vertically printed plates absorb less energy than the horizontal printed plates.

273 5.2 Uncertainties and error propagation in the analysis

274 To properly contextualize the experimental results presented, an analysis of the uncertainty and error
 275 propagation within the measurement chain was conducted. The final uncertainty provides a confidence
 276 range for the data and establishes a benchmark for the comparison of future test results.

277 The primary sources of uncertainty were identified as:

- 278 1) Manufacturing tolerance: The 3D printer's nozzle size introduces a thickness uncertainty of $\pm 0.8\text{mm}$,
 279 which is in line with tolerances for samples commonly produced in CFRP and was not considered a
 280 variable in this analysis. However, this tolerance contributes to the variability of the physical
 281 phenomenon rather than the measurement uncertainty, and it has been considered when evaluating
 282 the scatter in the final results
- 283 2) Projectile velocity: The light-gas gun's velocity measurement system has a declared sensitivity of $\pm 1\%$
- 284 3) Mass measurement: The uncertainty on mass measurements is 0.01g , which translates to a negligible
 285 relative uncertainty of approximately 0.01% for the single plates.
- 286 4) Video analysis calibration: The largest source of error comes from the video analysis, specifically the
 287 calibration of the pixel size. This was calibrated by measuring the known size of the plate in a frame
 288 and calculating the pixel-to-mm ratio. However, varying the binarization threshold for this
 289 measurement resulted in a slight variation in the calculated plate size, leading to a relative error of
 290 5% in the pixel dimensioning.

291 The total propagated uncertainty for parameters involving kinetic energy (E_k) and video analysis was
 292 calculated by combining the constituent errors.

293 Using kinetic energies, and thus multiplying the mass by the velocity squared, a conservative estimation of
 294 the error is derived from (2):

$$295 \text{Err}_{E_k} = 1 + 1 + 0,1 = 2,01\% \quad (2)$$

296 In video analysis, the uncertainty of the measurement is related to the uncertainty of the pixel size. This
 297 procedure was followed for calibration: a frame in which only the plate is visible was selected and was
 298 binarized according to a threshold, so as to have an image with white pixels for the background and black

299 pixels for the plate, for each row the number of black pixels was counted, a mathematical average of the
 300 number of rows was made to have an average size of the width

301 The actual size of the plate was then measured with a caliper and from the ratio of the measurements
 302 obtained, the pixel size was identified.

303 The uncertainty in this measurement is caused by the fact that depending on the threshold value selected,
 304 the average plate size calculated by the software may vary slightly. A relative error of 5% is obtained from
 305 the ratio of the calculated maximum and minimum plate dimensions

306 Combining all uncertainties quadratically produces a relative uncertainty value of:

$$307 \quad Err_{tot} = \sqrt{Err_{Ek}^2 + Err_{pixel}^2} = \sqrt{2,01^2 + 5^2} = 5,39\% \quad (3)$$

308 This the range of error, with a level of confidence of 95%, is to be kept for further testing in order to
 309 adequately compare future results.

310 It is noted that this value is dominated by the pixel calibration error. Future campaigns should include fixed
 311 reference markers in the experimental setup to allow for a more precise calibration and significantly reduce
 312 this component of the uncertainty.

313 **Conclusions**

314 This study successfully developed and demonstrated a methodology for the rapid prototyping of satellite
 315 protection shields using 3D-printed carbon fibre and Kevlar composites. While the preliminary test campaign
 316 was primarily intended to validate this methodology and the associated analysis techniques, several
 317 important conclusions can be drawn from the ten hypervelocity impact tests performed.

318 The results indicate that manufacturing parameters, particularly printing orientation, have a significant effect
 319 on ballistic performance. Horizontally printed single plates appeared to be more efficient in resisting impact
 320 than vertically printed plates, which were prone to delamination and fracture between layers under high-
 321 energy impacts. This suggests that while horizontal printing is superior, further investigation is needed to
 322 overcome the technological constraints of using this orientation to build multi-plate Whipple-type shields,
 323 possibly by developing novel support or filler structures. The quantitative analysis procedures developed in
 324 Matlab™ for measuring damage and debris cloud characteristics proved to be effective indicators for
 325 determining the energy absorbed by the shields and comparing the efficiency of different geometries.

326 Horizontal production of simples appears to be more efficient than vertical production, however, it is
 327 necessary to understand how to overcome the technological constraint in order to use it to create whipple-
 328 type shields, investigating the possibility of constructing support or filler structures.

329 In addition, image analysis procedures developed on Matlab™ can be used as a quantitative indicator to
 330 determine the energy absorbed by the shields and evaluate the efficiency of the geometries tested.

331 The main limitations of this initial campaign were the small number of tests and minor production
 332 inconsistencies between samples. Furthermore, the use of a single high-speed camera limited the debris
 333 cloud analysis to two dimensions, necessitating some assumptions and simplifications. The adoption of a
 334 second camera would allow the cloud to be studied in three dimensions and possibly to avoid saturation
 335 problem at the moment of impact.

336 Finally, in a future test campaign, these structures will be compared to standard structures used to protect
 337 satellites with the same weight to determine the real improvement these structures bring to spacecraft
 338 shielding.

339 **Acknowledgements**

340 The work described in this paper is partially carried out as part of the SBORAEK (R&I-2022-002L) project which
 341 was financed by Xjenza Malta, through the FUSION – Technology Development Programme LITE. This activity
 342 has been performed in the framework of a collaboration between the Center of Space Studies CISAS “G.
 343 Colombo” of the University of Padova and the Malta College of Arts, Science, and Technology (MCAST).

344 The authors would like to thank Thiot Ingegnerie for the assistance in hypervelocity testing and to SkyUp
345 Academy for the support.

346

347 **References**

348

- [1] A. K. Nervold, J. Berk, J. Straub and A. Whalen, "A Pathway to Small Satellite Market Growth," *Advances in Aerospace Science and Technology*, 2016.
- [2] F. Piergentili, N. Bellini, A. Locarini, S. Naldi, D. Rastelli, M. Valdatta and S. Bagassi, "Fused deposition modeling techniques for manufacturing of cubesat based on modular design concept," in *64th IAC*, Beijing, China, 2013.
- [3] L. Olivieri, C. Giacomuzzo, A. Francesconi, H. Stokes and A. Rossi, "Experimental characterization of multi-layer 3D-printed shields for microsatellites," *Journal of Space Safety Engineering*, vol. 7, no. 2, pp. 125-136, 2020.
- [4] B. N. Turner and S. A. Gold, "A review of melt extrusion additive manufacturing processes: II. Materials, dimensional accuracy, and surface roughness," *Rapid Prototyping Journal*, vol. 21, pp. 250-261, 2015.
- [5] J. T. Belter and A. Dollar, "Strengthening of 3D Printed Fused Deposition Manufactured Parts Using the Fill Compositing Technique," *PLoS One*, vol. 10, pp. 1-19, 2015.
- [6] L. Li, Q. Sun, C. Bellehumeur and P. Gu, "Composite Modeling and Analysis for Fabrication of FDM Prototypes with Locally Controlled Properties," *Journal of Manufacturing Processes*, vol. 4, no. 2, pp. 129-141, 2002.
- [7] ESA, "Annual Space Environment Report," 2025.
- [8] L. Olivieri, C. Giacomuzzo and F. Francesconi, "Experimental characterization of multi-layer 3D printed shields for microsatellites," in *69th IAC*, Bremen, Germany, 2018.
- [9] H. Hoshi, K. Nakano and Y. Iwahori, "Study on repair of CFRP laminates for aircraft structures,," in *16th International Conference on Composite Materials*, Kyoto, Japan.
- [10] R. Destefanis, E. Amerio, M. Briccarello, M. Belluco, M. Faraud, E. Tracino and C. Lobascio, "Space environment characterisation of Kevlar®: good for bullets, debris and radiation too," *Universal Journal of Aeronautical & Aerospace Sciences*, pp. 80-113.
- [11] A. Saleem, P. S. Ahmed and M. S. Abed, "Experimental and numerical investigation of Kevlar and UHMWPE multi-layered armors against ballistic impact," *Materials Today*, vol. 56, pp. 2516-2524, 2022.
- [12] R. Stevens, "Concurrent engineering methods and models for satellite concept design," in *IEEE Aerospace conference*, Montana, USA, 2015.
- [13] L. G. Blok, M. L. Longana, H. Yu and B. K. S. Woods, "An investigation into 3D printing of fibre reinforced thermoplastic composites," *Additive Manufacturing*, vol. 22, pp. 176-186, 2018.

- [14] S. Harder, F. Röper, D. Gibhardt, B. Koert and B. Fiedler, "Strength of scarf-bonded CFRP repairs containing disc-shaped zones of weak bonding considering hot-wet conditioning," *International Journal of Adhesion and Adhesives*, p. 102, 2020.
- [15] M. Mao, Z. Meng, X. Huang, H. Zhu, L. Wang, X. Tian, J. He, D. Li and B. Lu, "3D printing in space: from mechanical structures to living tissues," *International Journal of Extreme Manufacturing*, vol. 6, no. 2, 2024.
- [16] W. Wu, P. Geng, G. Li, D. Zhao, H. Zhang and J. Zhao, "Influence of layer thickness and raster angle on the mechanical properties of 3D-printed PEEK and a comparative mechanical study between PEEK and ABS," *Materials (Basel)*, vol. 8, p. 5834–5846, 2015.
- [17] A. Rossi and Al., "The H2020 ReDSHIFT project: a successful European effort towards space debris mitigation," in *70th International Astronautical Congress*, Washington D.C., USA, 2019.
- [18] L. Barilaro, L. Olivieri, M. Wylie, S. Zaninotto and M. Baldissera, "An overview on Smart Ballistic Optimization for Repair of Aerospace Exostructures using 3D printed Kevlar," in *74th IAC*, Baku, Azerbaijan, 2023.

349

350

Rapid Prototyping of Satellite Shields: 3D Printed Carbon Fiber and Kevlar Composites for Hypervelocity Impact Protection

Highlights

- Satellite shields are 3D printed in CFRP and Kevlar;
- Single Shield and Whipple Shield configuration were studied;
- 10+1 hypervelocity impact tests performed;
- Cratered and delamination analysis performed;
- Debris cloud video analysis performed.

Journal Pre-proof

Declaration of interests

The authors declare that they have no known competing financial interests or personal relationships that could have appeared to influence the work reported in this paper.

The authors declare the following financial interests/personal relationships which may be considered as potential competing interests:

Leonardo Barilaro reports financial support was provided by Xjenza Malta. If there are other authors, they declare that they have no known competing financial interests or personal relationships that could have appeared to influence the work reported in this paper.